

Optimal Waypoint Navigation for Underactuated Cruising AUVs

Kangsoo Kim

National Maritime Research Institute, National Institute of Maritime, Port, and Aviation Technology, 6-38-1 Shinkawa, Mitaka, Tokyo 181-0004, Japan

Keywords: Navigation, Waypoint, Optimization, Depth, Altitude, Cruising AUV, Bottom Collision.

Abstract: An advanced approach to the waypoint-based navigation for near-bottom survey of a cruising AUV is presented. Pursuing vehicle safety as well as high-definition bottom survey data, we apply GDS-based optimization technique for achieving waypoint-based minimum-altitude flight of an underactuated cruising AUV. While the objective of our optimization is minimizing average altitude of a vehicle throughout its flight interval, depth or altitude references on waypoints are used as control inputs. In our optimization, bottom bathymetry is incorporated as a constraint used for bottom collision avoidance. As another constraint, dynamic model of an AUV is included. By solving the dynamic model in time domain, motion responses of the vehicle following reference waypoints are derived. Our approach of the optimal waypoint navigation is validated by not only simulation but also at-sea deployment of an AUV.

1 INTRODUCTION

Providing far higher resolution bottom survey data than can be obtained from surface vessels, AUVs are increasingly being used in a diverse range of applications in the scientific, military, commercial, and policy sectors (Wynn et al., 2014). However, as its altitude from the bottom decreases, an AUV is faced with higher risk of bottom collision. The risk of bottom collision is especially serious when an underactuated vehicle exercises low-altitude flight over a steep and rugged terrain. It is common to classify AUVs into two categories according to their behavioral character: hovering and cruising (McPhail et al., 2010). It can be said that cruising AUVs are typically the choice for higher-speed, longer-range missions. In general, a hovering AUV can hover and maneuver around an operating point, while most cruising AUVs cannot. This is because most cruising AUVs are underactuated, and thus have restricted path-following capability (Lea et al., 1999). Due to this restriction, a cruising AUV has difficulty in avoiding impending collision with the obstacles in close proximity, which discourages it from flying over a steep and rugged terrain. Another concern of the flight of a cruising AUV over a steep and rugged terrain is that its onboard sonar altimeter is susceptible to so called "loss of bottom lock". Once occurs, the loss of bottom lock disables the use of

correct vehicle altitude, leading to the increased hazard of bottom collision (Keranen et al., 2012). In this paper, we demonstrate that the loss of bottom lock is especially favored by a bottom-following flight over a steep and rugged terrain. Unlike altitude, the depth of an underwater vehicle is highly accurate and reliable, being obtainable merely by measuring ambient water pressure. In this paper, we present depth-based optimal waypoint navigation as an alternative for the altitude-based acoustic navigation. By following the waypoints derived by GDS (gradient descent search)-based optimization, an AUV achieves minimum-altitude flight over a steep and rugged terrain avoiding bottom collision.

2 WAYPOINT NAVIGATION

In underwater vehicle navigation, waypoints are the set of 3D coordinates identifying the navigational points defined as the latitude, longitude, and depth or altitude pairs. Within the framework of waypoint navigation, a vehicle moves toward a destination passing through the reference waypoints. Figure 1 shows a sample of waypoints generated for AUV-based near-bottom survey of a submarine volcano. As shown, the reference path is spontaneously defined by the waypoints. In Fig. 1, it is noted that the numbers attached to each waypoint represent reference depths.

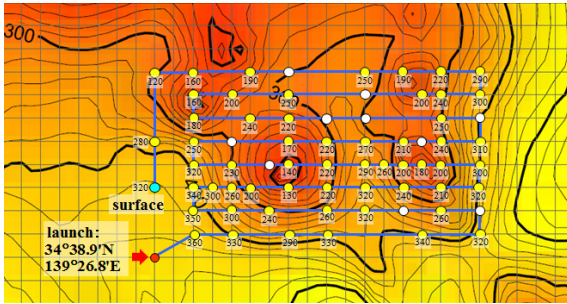


Figure 1: Waypoints and reference path generated for a near-bottom survey by an AUV.

In our waypoint-based navigation, the reference depth of n -th waypoint, (i.e. wp_n) shown in Fig. 1 is the desired depth to be reached by a vehicle during its transit between wp_{n-1} and wp_n . Therefore, no sooner has the vehicle arrived at wp_{n-1} , its target vertical position is updated to the reference depth of wp_n (Fig. 2). In Fig. 2, d_i and d_r are the current and the desired (reference) vehicle depths, while h_i and h_r are their altitude counterparts, respectively.

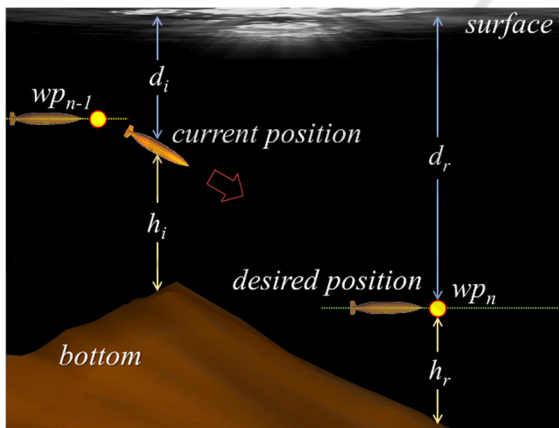


Figure 2: Waypoint-based depth control of an AUV.

It is to be noted here that instead of depth, altitude from the bottom also can be used for controlling the vertical position of an underwater vehicle. In our work, altitude means the absolute altitude in air navigation, i.e., the height of a vehicle above the terrain over which it is traversing (U.S. Air Force, 2005). The altitude control works on the basis of the altitude error e_h defined as the difference between the reference and the current altitude of a vehicle. It is noted that, however, by substituting the altitude error with its depth error counterpart, a depth controller is also able to exercise the altitude control equivalently. Hence, it is very common that a depth controller of an AUV is also in charge of the altitude control (McPhail et al., 2010; Kim and Ura, 2015). In such cases, we can recognize that for the altitude control

$$e_d = -e_h \quad (1)$$

where e_d is the depth error counterpart of the current vehicle altitude error $e_h = h_r - h_i$.

3 NEAR-BOTTOM SURVEY FLIGHT

Near-bottom survey of a seafloor is one of the most important AUV missions in its diverse applications. Being able to fly close to the bottom, AUVs are capable of collecting seafloor mapping, profiling and imaging data of far higher resolution and navigational accuracy than surface vessels (Wynn et al., 2014). However, moving close to the bottom inevitably raises the risk of bottom collision. This is especially serious when a cruising AUV is flying over a rugged and steep terrain keeping low altitude above the bottom.

3.1 Bottom Collision

Figure 3 illustrates the possible bottom collision of a cruising AUV during its waypoint-based near-bottom mission over a steep and rugged terrain.

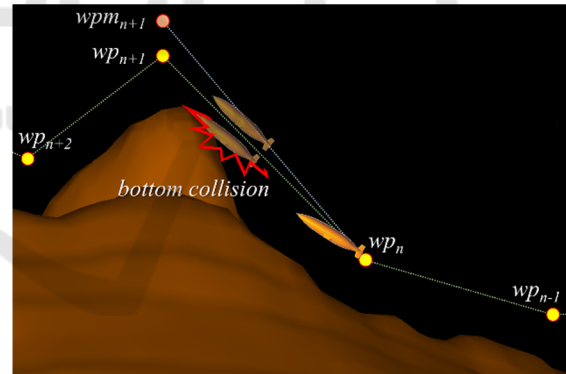


Figure 3: Bottom collision of an underactuated cruising AUV over steep and rugged terrain.

Suppose that the reference depth of any waypoint is merely assigned as the depth determined by an arbitrary constant altitude above the bottom. Then, although the reference path generated by interlinking adjacent waypoints runs over the seafloor without any interference with the terrain, an underactuated vehicle following the waypoints can cause a bottom collision (Fig. 3). This is because the reference path has been generated without considering the constraint of vehicle dynamics which can let the vehicle faced with too low altitude to avoid imminent bottom collision. In Fig. 3, bottom collision occurs within the path

interval between $[wp_n \sim wp_{n+1}]$. However, by modifying the reference depths of the waypoints within the interval, i.e., by substituting wpm_{n+1} for wp_{n+1} , for example, we can make the vehicle avoid bottom collision, as shown in the figure. As can be noticed from Fig. 3, in order to avoid bottom collision, the constraint of vehicle dynamics as well as the bottom topography should be considered.

3.2 Bottom-following Flight

As mentioned previously, altitude can be used in determining the vertical reference position of a vehicle. A typical example of such approach is the navigation so called bottom following (Caccia et al., 2003). In the bottom-following flight, a vehicle is controlled to follow the bottom maintaining a fixed altitude above it (Fig. 4). Thus, a device for measuring current vehicle altitude is essential for practicing a bottom-following flight. Most modern AUVs are equipped with a bottom-lock sonar such as DVL (Doppler Velocity Log) for this purpose.

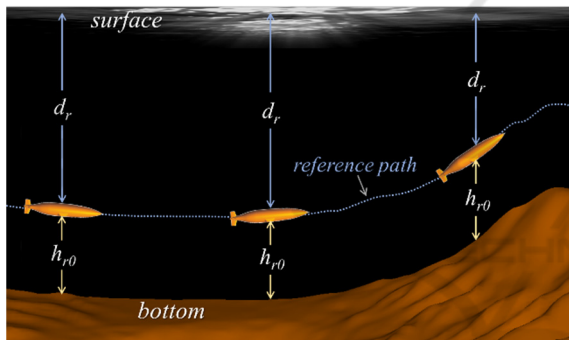


Figure 4: Bottom-following flight of a cruising AUV.

In Fig. 4, h_{r0} is the constant reference altitude assigned for a bottom-following flight. It is noted that while h_{r0} is constant, d_r changes according to current vehicle position. When the bottom-following flight works without fail, a vehicle exactly follows the reference path defined as the along-track bottom section parallelly shifted upward by h_{r0} (Fig. 4). In practice, however, the bottom following is not so reliable as the waypoint-based depth control because it relies entirely on real-time vehicle altitudes provided by a bottom-lock sonar.

4 ACOUSTIC NAVIGATION

In general, depth sensor installed in most modern AUVs is a quartz crystal pressure sensor calculating current vehicle depth from the direct measurement of

ambient seawater pressure. It is known that such pressure sensor provides very high precision whose accuracy of 0.01% of full scale (Kinsey et al., 2006). Therefore, it is noted that waypoint-based depth control is a highly reliable means for achieving stable and robust underwater vehicle navigation in vertical plane. As regards vehicle altitude, a bottom-lock sonar working on the basis of the single range acoustic time-of-flight navigation is used in estimating its current value above the bottom. Varying with the frequency of carrier signal, precision of echo sounding is said to be 0.01 ~ 1.0 m (Kinsey et al., 2006). The precision seems to be acceptable for near-bottom flight of a cruising AUV. However, there still is a serious concern in acoustic time-of-flight navigation. Altitude measurement by using a bottom-lock sonar system is highly vulnerable to the surrounding environment.

4.1 Altitude Overestimation

The first vulnerability of the altitude-based bottom-following flight of a cruising AUV is possible overestimation of the vehicle altitude over a steep terrain. As shown in Fig. 5, over a steep terrain, even a small change in vehicle's attitude may result in a large variation of indicated altitude. Suppose that a vehicle following the bottom is instantaneously taking large nose-up attitude when it has reached a steep downhill. Then, indicated altitude h_{m2} is used for ongoing bottom-following flight instead of h_{m1} , the true altitude. Since h_{m2} is largely overestimated compared to its true counterpart, the vehicle may try to approach the bottom further lowering its altitude even when h_{m1} is smaller than h_{r0} .

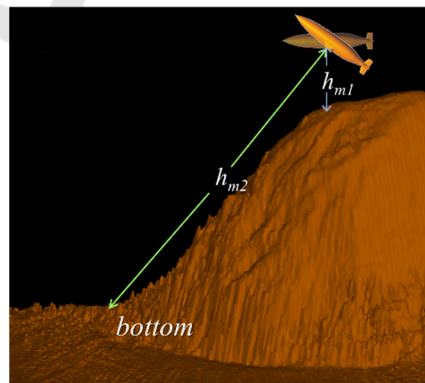


Figure 5: Indicated and true altitudes over a steep terrain.

4.2 Loss of Bottom Lock

In order for a bottom-lock sonar system to work properly, its receiver signal-to-noise ratio (SNR)

should be higher than the detectable limit called threshold SNR (Urlick, 1982). Since the acoustic energy projected by a transmitter dissipates due to the transmission losses, echoes show markedly reduced acoustic intensity from the source level (SL). Moreover, when a travelling acoustic wave encounters sea bottom leading to an echo event, some fraction of its energy is transmitted into the bottom. Dissipation in seawater and transmission into the sea bottom of acoustic energy are the major sources of reduced echo level (EL) lowering SNR (Urlick, 1982). When the EL of sonar echo is so small as for its SNR to be lower than the threshold value, a bottom-lock sonar is no longer able to lock on to the seafloor. This state is called "loss of bottom lock" in which any bottom-reference sonar observation is unavailable. Losing the information of current altitude, an underwater vehicle following a seafloor for near-bottom flight is faced with the serious risk of bottom collision when loss of bottom lock occurs.

5 MOTION INSTABILITIES

We experienced serious motion instabilities of a cruising AUV during its mission of surveying a submarine volcano called NW Rota-1. Figure 6 shows the AUV r2D4 having been deployed in NW Rota-1 site. The r2D4 is a cruising AUV developed by Institute of Industrial Science, the University of Tokyo (Kim and Ura, 2009). NW Rota-1 is an active submarine volcano, located in 64 km NW of the island of Rota in the western Pacific Ocean.

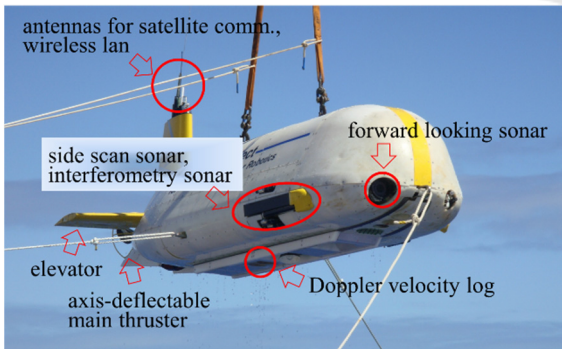


Figure 6: Overall layout of r2D4.

5.1 Control and Navigation

Figure 7 shows the schematic block diagram of depth control implemented in r2D4 (Kim and Ura, 2009). It is noted here that the duality mentioned above is applied to the depth and altitude control of r2D4. That is, it is the depth controller shown in Fig. 8 that

actually works corresponding to the altitude control exercised by bottom following.

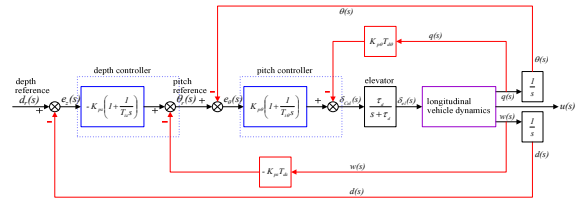


Figure 7: Block diagram of the depth control of r2D4.

In Fig. 7, e_z and e_θ are depth and pitch errors; θ_r and θ are reference and output pitch; d is vehicle depth; q is pitch rate; u and w are surge and heave velocities; and δ_{el} and δ_{cel} are elevator deflection and its command, respectively. K denotes controller gain while T derivative or integral time.

Figure 8 shows the navigation applied to r2D4 during its NW Rota-1 survey mission. In Fig. 8, AC is a part of the reference path generated for r2D4 flight #16. AC is called the "near-the-top" interval, generated for covering the area in the vicinity of the top of NW Rota-1. In flight #16, both constant depth flight and bottom following were used as the navigation for bottom survey. To the anterior section AB of the near-the-top interval, constant depth flight with the reference depth of 510 m was applied. Along the posterior section BC, on the other hand, vehicle was made to follow the bottom keeping its altitude 150 m off the bottom.

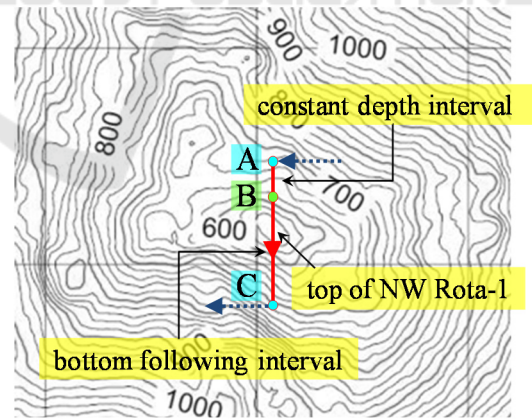


Figure 8: Navigation applied to near-the-top path interval.

5.2 Motion Instabilities over a Steep Terrain

Figure 9 shows the bottom cross section of NW Rota-1 taken along the near-the-top interval. Bottom bathymetry along a vehicle trajectory is obtained merely by summing the vehicle depth and the altitude

sequences. In the bottom cross section obtained, we find saw-teeth like, large and unnatural subsidence continuing along the descending terrain (Fig. 9).

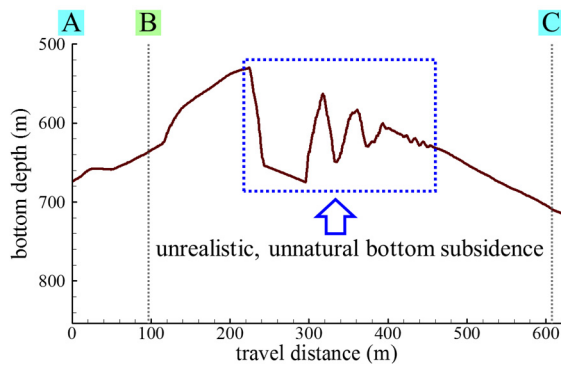


Figure 9: Vertical cross section of submarine volcano NW Rota-1 along near-the-top path interval.

Motivated by this too unrealistic shape of the bottom cross section, we checked the time sequences of vehicle's depth, altitude, and pitch taken from the log of r2D4 flight #16. Figure 10 shows depth and altitude sequences taken along the near-the-top path interval shown in Figs. 8 and 9.

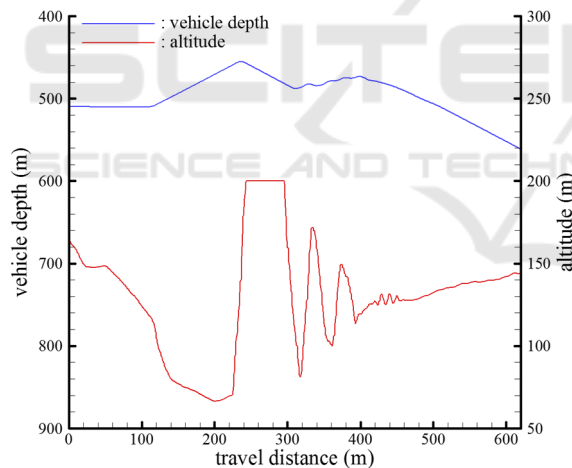


Figure 10: Vehicle depth and altitude.

In Fig. 10, we notice that while fluctuating slightly, the depth sequence seems normal, since its rate of change is reasonable within the normal range of the heave rate of r2D4. On the other hand, however, the altitude is definitely erroneous since the maximum value of its time derivative reaches 13.8 m/s which is more than 9 times the cruising speed of r2D4. Figure 11 shows pitch sequence of the vehicle together with its altitude counterpart. As can be expected from intrinsic heave-pitch coupling of a longitudinally asymmetrical slender body, vehicle's pitch also

fluctuates synchronizing with the altitude fluctuation. It is noted here that pitch fluctuates bounded within the range of -25° to 25° which are the predefined lower and upper limits of the pitch reference. Judging from its magnitude as well as rate of change, pitch does not show any notable abnormality.

Acknowledging that the measured vehicle depth is normal, we can conclude that it is erroneous vehicle altitude that is responsible for the unrealistic bottom cross section obtained.

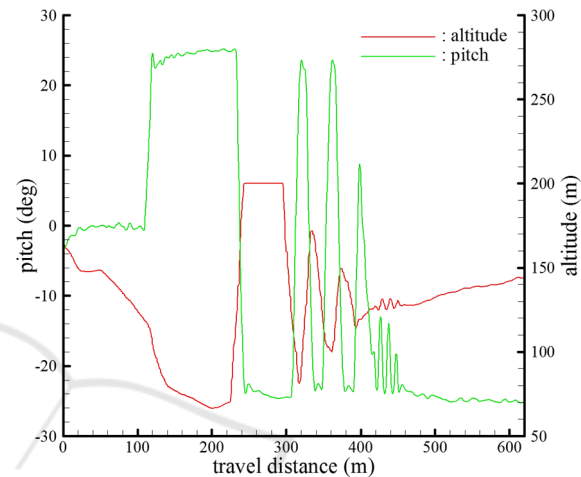


Figure 11: Pitch and altitude.

5.3 Acoustic Bottom Backscatter

If we apply the sonar equation (Urlick, 1983; Morgan, 1978; Miline, 1983) to our DVL altimeter, the echo level (EL) of returned signal is

$$EL = SL - 2TL + TS \quad (2)$$

where SL , TL , TS are the source level, the transmission loss, and the target strength, respectively. If NL denotes the noise level, we obtain the receiver SNR as follows.

$$SNR = EL - NL = SL - 2TL + TS - NL \quad (3)$$

In (3), energy loss arising from bottom scattering is expressed by means of the target strength (Morgan, 1978; Urlick, 1983). In an active sonar, the target strength is a measure of the reflecting power of a sonar target defined as

$$TS = 10 \log_{10} \frac{I_s}{I_i} \quad (4)$$

where I_i and I_s are the incident and the scattered acoustic intensities, respectively.

As the bottom is an effective reflector and scatterer of sound, it acts to redistribute a portion of the sound in

the ocean (Urlick, 1983). Not all of the sound is reflected or scattered, however, but some fraction of acoustic energy is transmitted into the bottom. The acoustic bottom backscatter is the reflection of sound on a sea bottom back to the direction from which it came (Fig. 12). Therefore, it is the backscattered sound that primarily activates a bottom-lock sonar. In case of acoustic bottom scatter, TS , the sonar target strength is frequently referred to as bottom strength. Also, it is well known that the bottom strength directly depends on the incidence angle of impinging acoustic ray. More precisely, providing the maximum strength at normal incidence, i.e., zero incidence angle, the bottom strength decreases notably as the incidence angle increases (Urlick, 1983; Moustier and Alexandrou, 1991).

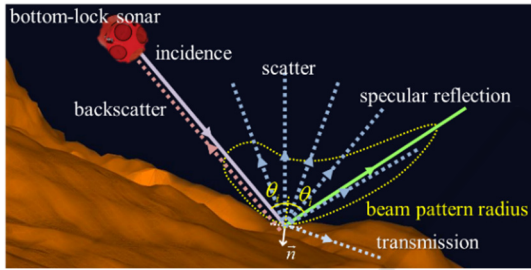


Figure 12: Sound redistribution on the bottom by the impinging acoustic ray of incidence angle θ .

It is well known that bottom strength is also dependent on the sound frequency of impinging acoustic ray (Mackenzie, 1961; Urlick, 1983). In r2D4, a 300 kHz, 4-beam DVL is used as altimeter. Li et al. (2012) presents a smooth curve of 300 kHz bottom acoustic backscatter as a function of incidence angle (Fig. 13). By using the curve, we can easily evaluate I_s corresponding to any incidence angle on the bottom.

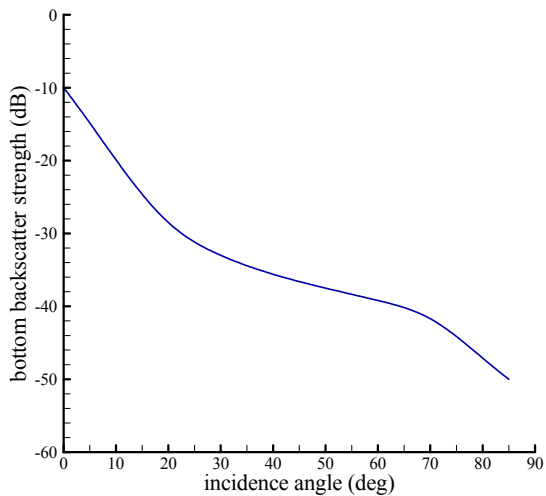


Figure 13: Bottom backscatter strength of 300 kHz sound.

It is officially announced that the source level and the maximum range of our DVL are 216.3 dB and 200 m, respectively (Teledyne RD Instruments, 2013). This enables us to estimate the threshold SNR of our DVL altimeter to be 35.7 dB (Kim and Ura, 2015).

Transmission loss in (2) and (3) can be calculated by

$$TL = TL_{sp} + TL_{at} = 20 \log_{10} R + \alpha R \quad (5)$$

where TL_{sp} and TL_{at} are the spherical spreading and the attenuation, respectively which are two major components of the transmission loss experienced by an acoustic signal travelling in a fluid medium (Morgan, 1978; Urlick, 1983; Miline, 1983). In (5), R is the distance from the source and α is the logarithmic absorption coefficient relating the signal intensity to range (Urlick, 1983).

For the noise level, we consider external background noise only ignoring cross-sensor acoustic interference. This is because in general, an AUV employs multiple sonars of totally different operating frequencies (Edward et al., 2007), and so does r2D4. It is noted that at the frequencies over 50 kHz, thermal noise begins to dominate the underwater background noise (Urlick, 1984). In evaluating the thermal noise level denoted as NL_{th} , we use the following relation (Mellen, 1952)

$$NL_{th} = -15 + 20 \log_{10} f \quad (6)$$

where f is the frequency of interest in kHz.

5.4 Simulated Bottom-following Flight

By using the mathematical model of underwater acoustics given as (2) ~ (6) and the vehicle dynamics of r2D4 (Kim and Ura, 2009), the near-bottom flight of r2D4 following the path interval AC (Fig. 9) has been simulated. All conditions of the simulation, e.g., the sea bottom topography, the flight path, and the navigation were taken from the r2D4 flight #16 mentioned above. Figure 14 shows the time history of simulated vehicle altitude. In Fig. 14, altitude log of the actual flight is superposed on the simulated result. As seen, like the actual flight, the simulation also demonstrates severely fluctuating vehicle motion. Moreover, as in the case with the actual flight, the largest altitude peak comes first followed by the gradually decaying smaller peaks. Figure 15 shows the simulated vertical cross section of NW Rota-1 along the interval AC. The flight simulation generates the same pattern of the bottom cross section as was obtained from the actual flight. Simulated vehicle pitch and the pitch log of the actual flight are shown in Fig. 16. Over the whole, it is noted that the vehicle

behaviors and the along-track bottom bathymetry obtained by the simulation show intrinsic similarities to those taken from the actual flight.

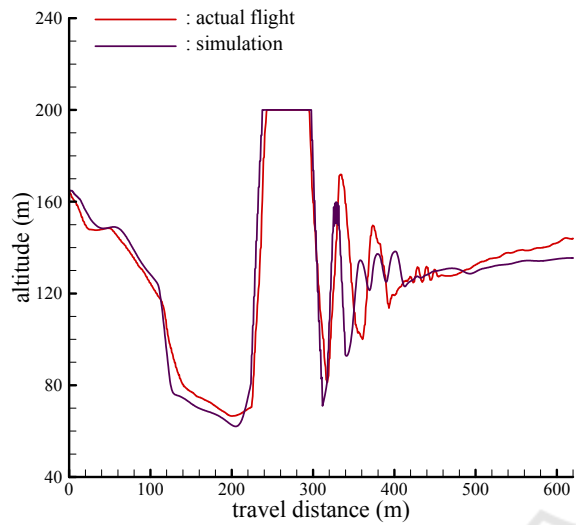


Figure 14: Simulated and actual vehicle altitudes.

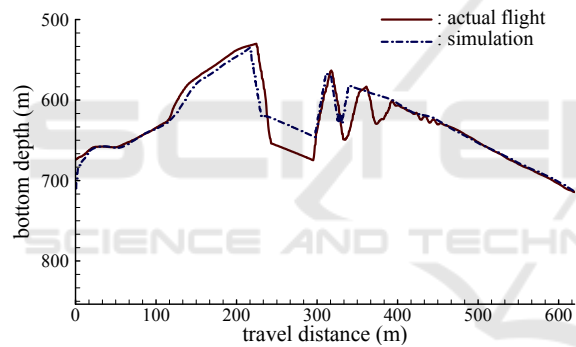


Figure 15: Simulated and actual bottom cross sections.

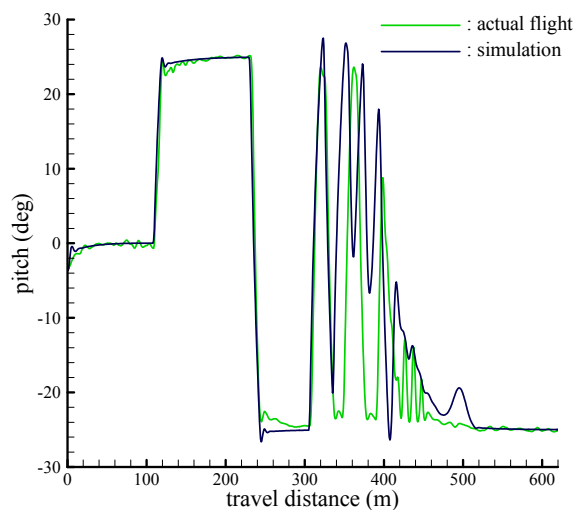


Figure 16: Simulated and actual vehicle pitch.

6 ALTERNATE NAVIGATION

6.1 Vulnerability of Acoustic Navigation

In the previous section, bottom-following flight simulation has reproduced the longitudinal motion instabilities of a cruising AUV r2D4 having been experienced during its actual near-bottom mission. In the previous literature by the author, a probable scenario explaining the generating mechanism of the motion instabilities are presented (Kim and Ura, 2015). In this scenario, the loss of bottom lock of DVL altimeter and the altitude overestimation are identified as two major sources inducing instabilities in longitudinal vehicle motion. Figure 18 shows the receiver SNR of our 300 kHz DVL altimeter derived from the flight simulation shown above. As already mentioned, a bottom-lock sonar gets trapped into the loss of bottom lock when the receiver SNR is lower than its threshold. By comparing Fig. 15 to 17, we can find that a sharp reduction in receiver SNR happens when the vehicle is about to pass through the top of NW Rota-1. And from Figs. 16 and 17, we notice that the interval in which the receiver SNR drops below its threshold nearly coincides with that of the first peak of altitude fluctuation. Thus, it is natural to infer that the large reduction in SNR is the direct source of the first peak in altitude fluctuation.

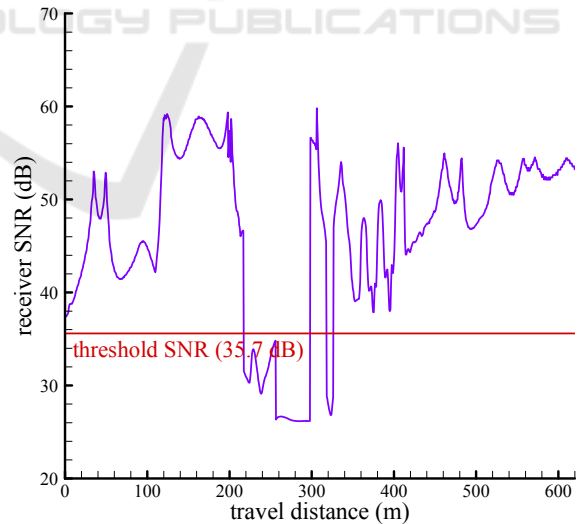


Figure 17: Simulated receiver SNR of DVL altimeter.

The reason of the sharp reduction in receiver SNR can be explained by the abrupt increase in acoustic incidence angle on the bottom near the top of the mountain. In order to follow an ascending terrain, a cruising AUV has to get nose-up. For a bottom-lock

sonar, nose-up over an ascending terrain forms a favorable operating condition, making incidence angle small. Approaching the top of the mountain with nose-up, however, makes the insonification switched to descending terrain which leads to abrupt increase in acoustic incidence angle (Fig. 18). Since backscattered bottom strength weakens remarkably as the bottom incidence angle increases (Fig. 13), switched insonified area is thought to be the cause of the sharp drop in receiver SNR, and eventually the loss of bottom lock.

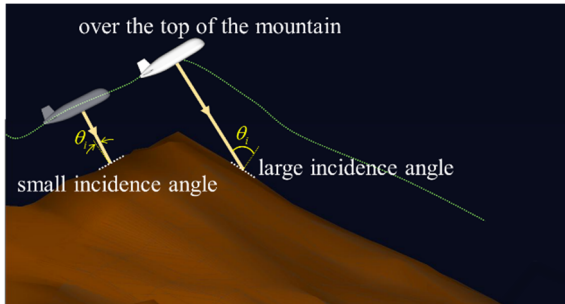


Figure 18: Switched insonified area.

Although the generation of the first altitude peak can be well explained by the sudden drop of receiver SNR, others cannot. In Fig. 17, we see whereas the altitude continues to fluctuate, there is only one significant SNR drop after 300 m of travel distance. As the reason that r2D4 continued nodding motion even after the extinction of significant SNR drop, we take notice of the large variation in measured altitude over a steep terrain. After recovering from the loss of bottom lock, r2D4 pitches nose up over steep descent, resulting in altitude overestimation. Once a cruising AUV gets a largely overestimated altitude, it unduly pitches nose down, in turn, in order to reduce the exaggerated altitude immediately. In our scenario, the repeated nose ups and nose downs, i.e., the nodding motion, of excessive magnitude triggered by the loss of bottom lock is the substance of motion instabilities appearing irrespective of the SNR drop (Fig. 19).

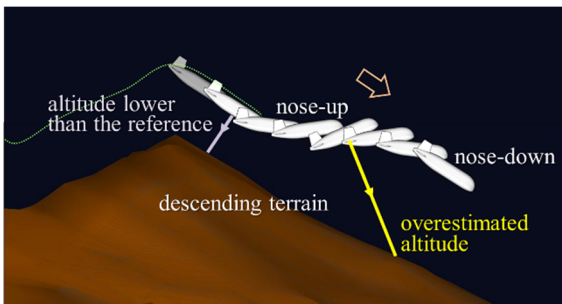


Figure 19: Repetitive nodding motion of a cruising AUV due to altitude overestimation.

6.2 Depth-based Navigation

As noticed from the simulation results shown above, altitude-based acoustic navigation for a cruising AUV has serious vulnerability to uneven bottom of steep slope. When the motion instabilities explained so far are detected during a near-bottom flight, it indicates that the vehicle is currently exposed to a significant hazard, since the occurrence of motion instabilities implies that the vehicle is blind to its true altitude. Furthermore, if the reference altitude is particularly low, e.g., below tens of meters, the motion instabilities put the vehicle at higher risk of bottom collision. Therefore, in order to circumvent the risk of bottom collision, more sophisticated navigation strategy for near-bottom flight is required.

As already mentioned, the measured depth of an underwater vehicle is far more reliable and accurate compared to the measured altitude. Therefore, being fundamentally free from the vulnerability to uneven and steep terrain, depth-based navigation ensures stable vehicle motion. Most depth-based navigation is put into practice by means of waypoints. Controlling actual vehicle trajectory, in practice, determining reference depths on waypoints is highly important for waypoint-based navigation. It is not easy, however, for us to derive the reference waypoint depth which produces the best performance in carrying out an assigned mission.

6.3 Waypoints for Minimum Altitude

The definition of optimal waypoints differs according to individual AUV flight missions. At present, it is widely accepted that high-resolution bottom survey is one of the most important and anticipative expectations for AUV flight missions (Wynn et al., 2013). In fact, the author's institute, National Maritime Research Institute (NMRI) of Japan also developed four cruising AUVs for high-resolution survey of submarine hydrothermal sites (Kim and Tamura, 2016). Considering these, we regard high-resolution bottom survey as the major mission of our AUV applications. Pursuing high-resolution bottom survey, an AUV has to travel in as close proximity to terrain as possible. Therefore, our optimal waypoints are defined as those accomplishes the minimum-altitude flight of an AUV. Figure 20 describes the basic concept of our approach. By following the optimal waypoints, an AUV conducts a near-bottom flight minimizing the average altitude along its flight path. In Fig. 20, h_a is the minimum allowable altitude within the flight path interval. It is noted here that h_a

should be identical to the lowest (i.e., minimum) altitude actually marked within the interval.

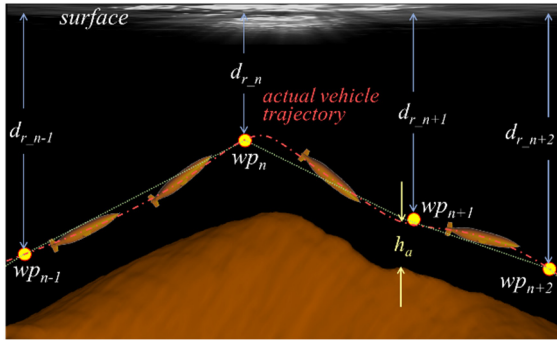


Figure 20: Minimum-altitude flight accomplished by following optimal waypoints.

6.4 Problem Formulation

To treat the problem of optimal waypoint navigation, two sets of coordinate system are employed: the inertial (earth-fixed) coordinate system $o-xz$ and the body-fixed coordinate system $o-x'z'$ (Fig. 21). While waypoint optimization is carried out with respect to the inertial frame, the motion response of a vehicle is calculated using the equation of motion defined with respect to the body-fixed frame.

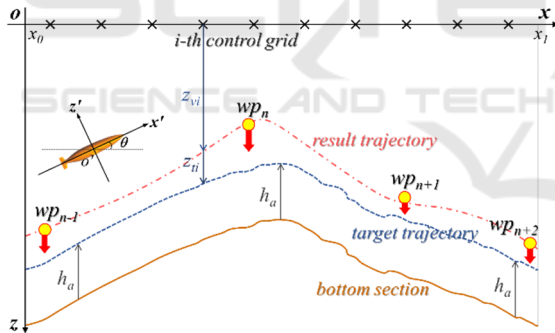


Figure 21: Coordinate systems and schematic description of the optimal waypoint derivation.

As already mentioned, the objective of our optimal waypoint navigation problem is to derive the waypoint set that minimizes average vehicle altitude along a given flight path. Therefore, the performance index of the problem is

$$J = \frac{1}{2} \int_{x_0}^{x_1} h^2(x) dx \quad (7a)$$

subject to

$$h(x) \geq h_a \quad \text{for } x \in [x_0, x_1] \quad (7b)$$

where $h(x)$ is the vehicle altitude at a specified along-track position x . In (7b), x_0 and x_1 are the along-track coordinates of the lower and the upper limits of the flight path interval of interest, and h_a is the minimum allowable altitude. It is obvious that once the minimum allowable altitude h_a is given, the ideal behavior of a vehicle is to follow the bottom throughout with its altitude of h_a . Hence, the target trajectory for optimizing the waypoints are given as the envelope line of the bottom section shifted upward (i.e., in $-z$ direction) by h_a , as shown in Fig. 21. In consequence, our problem results in the optimization making the deviation between the target and the result trajectories as small as possible. Let us introduce so called "control grid" represented by the cross symbol in Fig. 21. The control grid is a set of arbitrarily spaced discrete points on x -axis at which the deviation between the target and the result trajectories is evaluated. Accordingly, by using the control grid the performance index (7a) can be redefined as

$$J = \frac{1}{2} \|z_t - z_v\|^2 \quad (8)$$

where z_t and z_v are the downrange position vectors of the target trajectory and the vehicle defined at control grids. Note that in this paper, variables in boldface type denote vector or matrix. As already mentioned, we use a GDS-based solution algorithm in minimizing the performance index J in (8). In deriving the solution, our algorithm works in an iterative manner (Kim et al., 2011). By applying the algorithm, the downrange position vector of the waypoints is updated as

$$z_w^i = z_w^{i-1} + \Delta z_w \quad (9)$$

where z_w^i is the downrange position vector of the waypoints at i -th iteration step, estimated by adding Δz_w to z_w^{i-1} . In (9), Δz_w is the correction amount of z_w computed by

$$\Delta z_w = \eta \frac{dz_w}{d\tau} = -\eta [(z_v - z_t)G]^T \quad (10a)$$

where

$$G = \frac{dz_v}{dz_w} \quad (10b)$$

In (10a), η is the gain and τ is the non-physical variable for the fictitious dimension of iteration. It is noted that G is the Jacobian matrix of z_v with respect to the input vector z_w .

7 RESULTS

The efficacy of waypoint-based minimum-altitude navigation was validated through an actual near-bottom survey mission using an AUV. In 2018, we deployed an AUV called C-AUV#04 (Fig. 22) in a potential hydrothermal vent site located in western Pacific Ocean near Japan. C-AUV#04 is a high maneuverability cruising AUV developed by NMRI of Japan, having controllable pitch range of $\pm 80^\circ$ (Kim et al., 2019). C-AUV#04 controls its flight attitude by deflecting four movable fins mounted on the stern (Fig. 22). It is noted that two horizontal fins function as elevator and ailerons, while two vertical fins as rudder. As for the depth or altitude control, C-AUV#04 shares the same scheme of r2D4 explained in section 5.1.

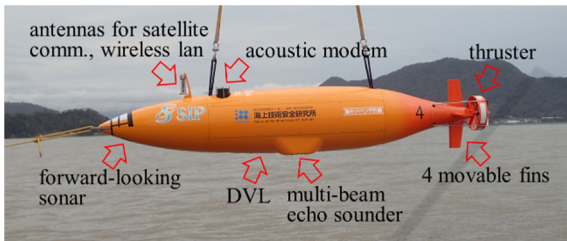


Figure 22: Overall layout of C-AUV#04.

When planning the path for C-AUV#04 flight #02 conducted for the near-bottom survey of the site, we derived optimal reference depths for the waypoints constituting the path interval covering western slope of a sea mound. Figure 23 shows the waypoints with their path interval superimposed on the bathymetric map of the site. As seen, fourteen waypoints are to be optimized in order to accomplish a depth-based, minimum-altitude flight along the path.

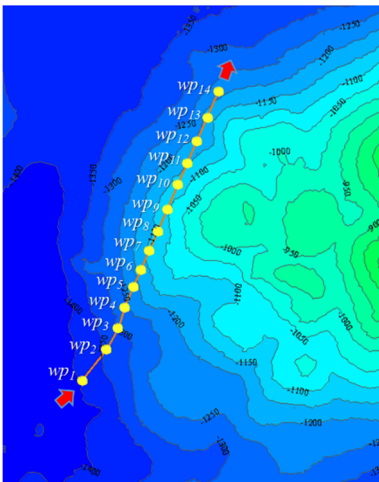


Figure 23: Waypoints and path interval.

The results of near-bottom survey flight following optimal waypoints are shown in Fig. 24. In optimizing the waypoints, we assigned the initial values of their reference depths with the water depths at the points 120 m above the bottom (Fig. 24). And it is also noted that the minimum allowable altitude is set to 80 m.

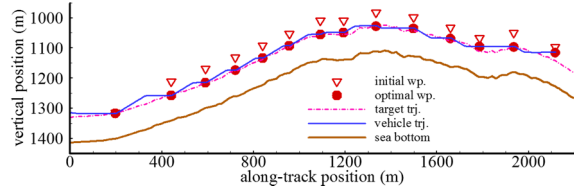


Figure 24: Results of minimum-altitude flight.

By modifying the waypoints, the GDS-based solution algorithm shifts the result trajectory away from the initial waypoints lowering vehicle altitudes within the flight path interval. Once a vehicle altitude derived by the flight simulation reduces to around the minimum allowable altitude, our algorithm terminates waypoint modification and outputs current waypoint set as the optimal solution. In this example, we can see small overshoots in descending intervals, but the vehicle successfully approaches the target trajectory, as a whole (Fig. 24). Since they are quite close to the minimum allowable altitude, the minimum altitudes let the solution algorithm terminate waypoint modification and take current waypoints as the optimal waypoints for the minimum-altitude flight. Uploaded to onboard storage device, derived optimal waypoints are used for the near-bottom survey mission. As can be seen in Fig. 24, by following the optimal waypoint set derived by our simulation-based approach, C-AUV#04 is able to complete near-bottom survey mission successfully.

8 CONCLUSIONS

A systematic procedure for deriving optimal waypoints used for AUV navigation has been presented. Using GDS-based optimization, the procedure derives optimal waypoints by following which an underactuated cruising AUV accomplishes minimum-altitude flight avoiding bottom collision. Being a depth-based approach, the optimal waypoint navigation is highly robust and fundamentally free from the vulnerability of acoustic navigation. It is a pregenerative approach, however, that requires the real time revision of optimal waypoints in case the vehicle is largely deviated from the planned path.

ACKNOWLEDGEMENTS

This work is partly supported by Council for Science, Technology and Innovation (CSTI), cross-ministerial Strategic Innovation Promotion Program (SIP), next-generation technology for ocean resources exploration (lead agency: JAMSTEC). Also, the author would like to express special thanks to Japan Marine Surveys Association (JAMSA) and Mr. Takumi Sato of National Maritime Research Institute (NMRI) of Japan, for their supports in AUV operation.

REFERENCES

- Wynn, B., Russel et al. (2014). Autonomous Underwater Vehicles (AUVs): Their past, present and future contributions to the advancement of marine geoscience. *Marine Geology*, 352 (2014), 451–468.
- McPhail, S., Furlong, M., and Pebody, M. (2010). Low-altitude terrain following and collision avoidance in a flight-class autonomous underwater vehicle. *Journal of Engineering for the Maritime Environment*, 224 (4), 279–292
- Lea, R. K., Allen R., and Merry S. L. (1999). A comparative study of control techniques for an underwater flight vehicle. *International Journal of System Science*, 30 (9), 947–964.
- Keranen, J. et al., (2012). Remotely-operated vehicle applications in port and harbor site characterization: Payloads, platforms, sensors, and operations. *Proc. of IEEE Oceans 2012 Hampton Roads*.
- U.S. Air Force (2005). *Air navigation*. University Press of the Pacific, Honolulu, ISBN 978-1410222466.
- Kim, K. and Ura, T. (2015). Longitudinal motion instability of a cruising AUV flying over a steep terrain, *IFAC-PapersOnline*, vol.48, issue 2, 56–63.
- Caccia, M., Bruzzone, G., Veruggio, G. (2003). Bottom-following for remotely operated vehicles: Algorithms and experiments. *Autonomous Robots*, 14, 17–32.
- Kinsey, J.C., Eustice, R.M., Whitcomb, L.L. (2006). A survey of underwater vehicle navigation: Recent advances and new challenges. *Proc. of 7th IFAC Conference on Manoeuvring and Control of Marine Craft*.
- Urlick, R.J. (1983). *Principles of underwater sound (3rd edition)*. McGraw-Hill, New-York, ISBN 0-07-066087-5.
- Kim, K., and Ura, T. (2009). Optimal guidance for autonomous underwater vehicle navigation within undersea areas of current disturbance. *Advanced Robotics*, 23 (5), 601–628.
- Morgan, M.J. (1978). *Dynamic Positioning of Offshore Vessels*, PPC Books Division, ISBN 0-87814-044-1.
- Miline, P.H. (1983). *Underwater Acoustic Positioning Systems*, E. & F. N. Spon Ltd, ISBN 0-419-12100-5.
- Moustier, C.D., and Alexandrou, D. (1991). Angular dependence of 12-kHz seafloor acoustic backscatter. *J. Acoust. Soc. Am.*, 90(1), 522–531.
- Mackenzie, K.V. (1961). Bottom reverberation for 530 and 1030 cps sound in deep water. *J. Acoust. Soc. Am.*, 33, 1498–1504.
- Li, M.Z., Sherwood, C.R., and Hill, P.R. (ed.) (2012). *Sediments, Morphology and Sedimentary Processes on Continental Shelves: Advances in technologies, research and applications*, Wiley-Backwell.
- Edward, T., James, R., and Daniel, T. (2007). Integrated control of multiple acoustic sensors for optimal seabed surveying. *IFAC Proceedings Volumes*, vol.40, issue 17, 367–372.
- Urlick, R.J. (1984). *Ambient noise in the sea*. University of Michigan Library, ASIN: B003U4V052.
- Mellen, R.H. (1952). Thermal-noise limit in the detection of underwater acoustic signals. *J. Acoust. Soc. Am.*, 24(5), 478–480.
- Teledyne RD Instruments, Inc. (2013). *Navigator Doppler velocity log technical manual*. Teledyne RD Instruments, Inc.
- Kim, K. and Tamura, K. (2016). The Zipangu of the Sea project overview: focusing on the R&D for simultaneous deployment and operation of multiple AUVs. *Proc. of OTC-Asia 2016*, OTC-26702-MS.
- Kim, K. and Ura, T., Kashino, M., and Gomi, H. (2011). A perioral dynamic model for investigating human speech articulation. *Multibody System Dynamics*, 26(2), pp.107-134, DOI: 10.1007/s11044-011-9253-z.
- Kim, K., Sato, T., and Matsuda, T. (2019). Advanced AUV navigation and operation towards safer and efficient near-bottom survey. *Proc. of MTS/IEEE OCEANS 2019 Marseille* (to appear).